

On-chip single photon emission from a waveguide-coupled two-dimensional semiconductor

Carlos Errando-Herranz,^{*,†,¶} Eva Schöll,^{*,†,¶} Micaela Laini,[‡] Samuel Gyger,[†] Ali
W. Elshaari,[†] Art Branny,[†] Ulrika Wennberg,[†] Sebastien Barbat,[†] Thibaut
Renaud,[†] Mauro Brotons-Gisbert,[‡] Cristian Bonato,[‡] Brian D. Gerardot,[‡] Val
Zwiller,[†] and Klaus D. Jöns^{*,†}

[†]*Quantum Nanophotonics, KTH Royal Institute of Technology, Roslagstullsbacken 21,
10691 Stockholm, Sweden*

[‡]*Institute for Photonics and Quantum Sciences, SUPA, Heriot-Watt University, Edinburgh
EH14 4AS, UK*

[¶]*Equal contribution*

E-mail: carloseh@kth.se; escholl@kth.se; klausj@kth.se

Abstract

Large-scale optical quantum technologies require on-chip integration of single-photon emitters with photonic integrated circuits. A promising solid-state platform to address this challenge is based on two-dimensional (2D) semiconductors, in particular tungsten diselenide (WSe_2), which host single-photon emitters that can be strain-localized by transferring onto a structured substrate. However, waveguide-coupled single-photon emission from strain-induced quantum emitters in WSe_2 remains elusive. Here, we use a silicon nitride waveguide to simultaneously strain-localize single-photon

emitters from a WSe₂ monolayer and to couple and transmit the emitted single photons. We demonstrate single-photon emission and waveguide coupling by measuring second-order autocorrelation of $g^{(2)}(0) = 0.150 \pm 0.093$ through the on-chip waveguide. Our results illustrate the potential of coupling emitters hosted by 2D semiconductors with photonic integrated circuits, paving the way towards large-scale optical quantum technologies.

Large-scale on-chip quantum technologies are crucial to realize the long-standing goals of quantum information processing, such as quantum computing based on cluster state generation,¹ quantum simulation,² and quantum communication.^{3,4} A promising route towards large-scale quantum information processing relies on single-photon qubits interconnected via photonic integrated circuits (PICs).⁵

Single-photon emitter integration into PICs has been achieved by embedding quantum dots into III-V PIC platforms,⁶⁻⁹ with limited scalability due to their optical loss, large waveguide bend radius, and low fabrication yields. To utilize the scaling offered by PICs, pick-and-place techniques have been developed to integrate III-V semiconductor quantum dots¹⁰⁻¹² and diamond color centers¹³ into silicon (Si) and silicon nitride (SiN) waveguide platforms. A drawback of this approach lies on the stringent requirements for emitter fabrication and precise pick-and-place of individual emitters, which drastically limit the scalability of this technology.

A promising candidate to overcome the current scalability limitations of quantum PICs is based on two-dimensional (2D) materials.^{14,15} In particular, transition metal dichalcogenides (TMDs)¹⁶⁻²¹ may enable hundreds of single-photon emitters by a single pick-and-place transfer using localized strain.^{22,23} Efforts towards 2D TMD single-photon emitter integration into PICs included transfer of a tungsten diselenide (WSe₂) monolayer on the facet of a titanium-indiffused lithium niobate waveguide with a large mode size,²⁴ and transfer on top of a lossy plasmonic slot waveguide.²⁵ More scalable approaches include coupling of single-photons from a gallium selenide layered semiconductor into SiN waveguides,²⁶ pho-

toluminescence from a WSe₂ monolayer into a SiN waveguide,²⁷ and emission from hexagonal boron nitride (hBN) into an aluminum nitride waveguide.²⁸ However, to prove the scaling prospects of this technology for on-chip quantum information processing, strain-localization of emitters and single-photon transmission through PIC waveguides is required, and still remains elusive.

Here, we use a Si₃N₄ PIC waveguide to simultaneously strain-localize single-photon emitters in a WSe₂ monolayer and to couple and transmit the emitted single-photons. Our results show the potential of combining 2D semiconductors with PICs towards large-scale quantum technologies.

Figure 1a shows a schematic of our sample, consisting of a U-shaped Si₃N₄ waveguide on a SiO₂ bottom cladding. The designed waveguide geometry supports the fundamental quasi-TE and quasi-TM waveguide modes as shown in figure 1b & c. The microscope image in Fig. 1d gives an overview of the whole structure, with cleaved facets and an exfoliated WSe₂ monolayer (1L) placed on top of the waveguide using a dry-transfer method²⁹ (see Fig. 1e and Supplementary). Figure 1f shows photoluminescence from emitters in the sample under de-focused excitation, recorded using a CCD camera with a 700 nm long pass filter to remove backscattered laser light. The measurements were performed with a modular setup consistent of a closed-cycle cryostat at 6 K where the sample was placed on a piezoelectric movable stage, a spectrometer, and a Hanbury Brown and Twiss (HBT) second-order correlation measurement setup, as shown in Fig. 2a. A more detailed explanation of the setup is given in the Supplementary. The emitters in the monolayer were excited from the top through a microscope objective with a red pulsed laser (638 nm) with variable repetition rate of 5-80 MHz. In line with reported strain-localization of single-photon emitters,^{22,23} we observe two lines of localized emitters along the waveguide edges. Since the flake remains continuous across the waveguide and shows no signs of rupturing or wrinkling, we expect that waveguide roughness along the edges is responsible for creating local strain potentials that localize the emission.

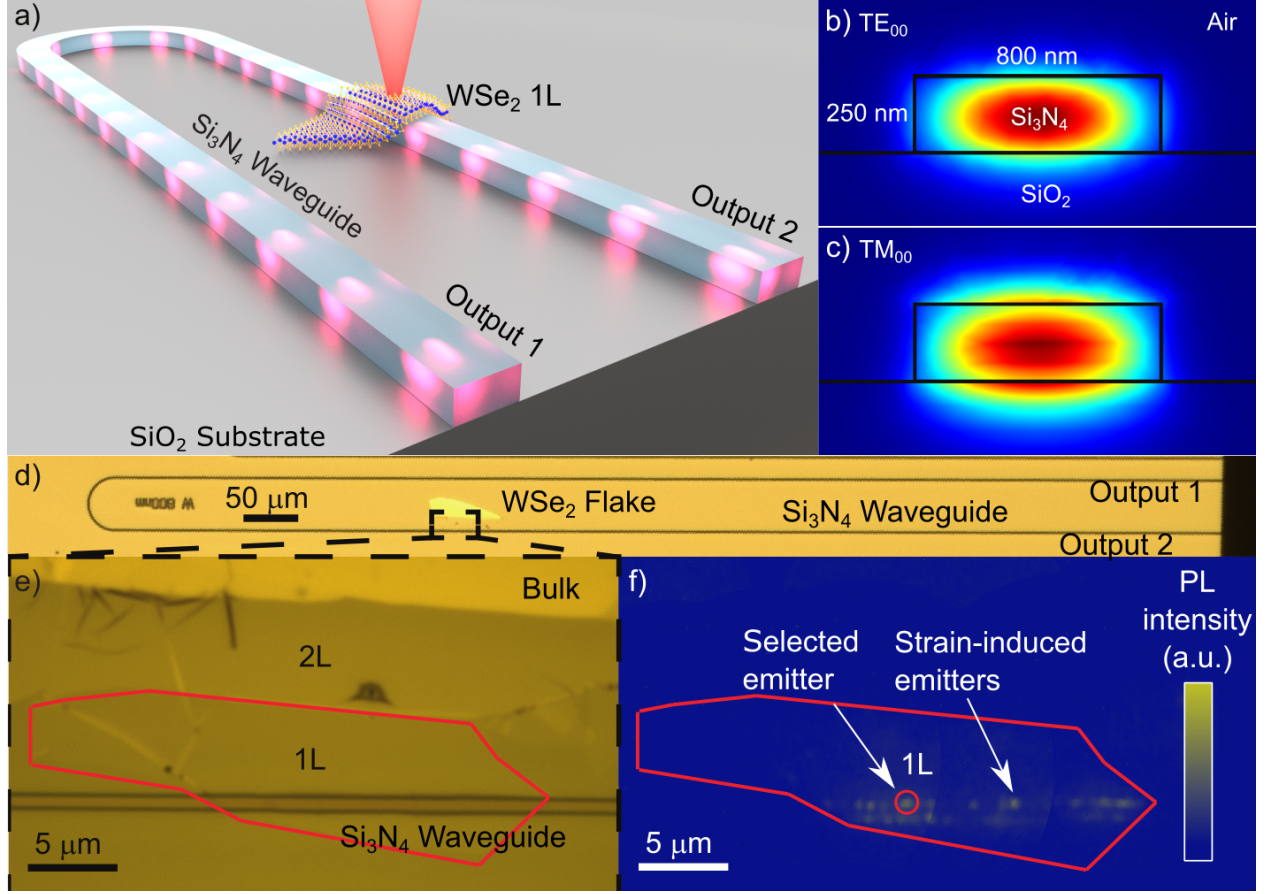


Figure 1: a) Artistic illustration of the coupled WSe₂ monolayer (1L) single-photon emitter and the Si₃N₄ waveguide. b) Finite element method eigenmode simulation of the fundamental quasi-TE and c) quasi-TM waveguide modes. d) Microscope image of the Si₃N₄ waveguide with e) zoom in of the WSe₂ flake. The monolayer is marked in red (1L). f) Photoluminescence with de-focused excitation shows strain-localized emitters along the waveguide edges. The emitter used for further experiments is marked with a red circle.

By focusing the excitation laser onto the sample and using a confocal microscopy setup, we recorded the photoluminescence spectra of single emitters. Figure 2b shows the spectrum of the emitter marked in Fig. 1f collected out of plane of the waveguide through the objective (top detection). Figure 2c and d show the spectra of the same emitter collected through the two waveguide output ports. The line at 770 nm of this emitter is used for all further measurements. A common signature of a two-level system is saturation of the emission intensity with increasing excitation power, shown in Fig. 3a in a double-logarithmic plot. Fitting the data as described in the Supplementary, we extracted a saturation power of

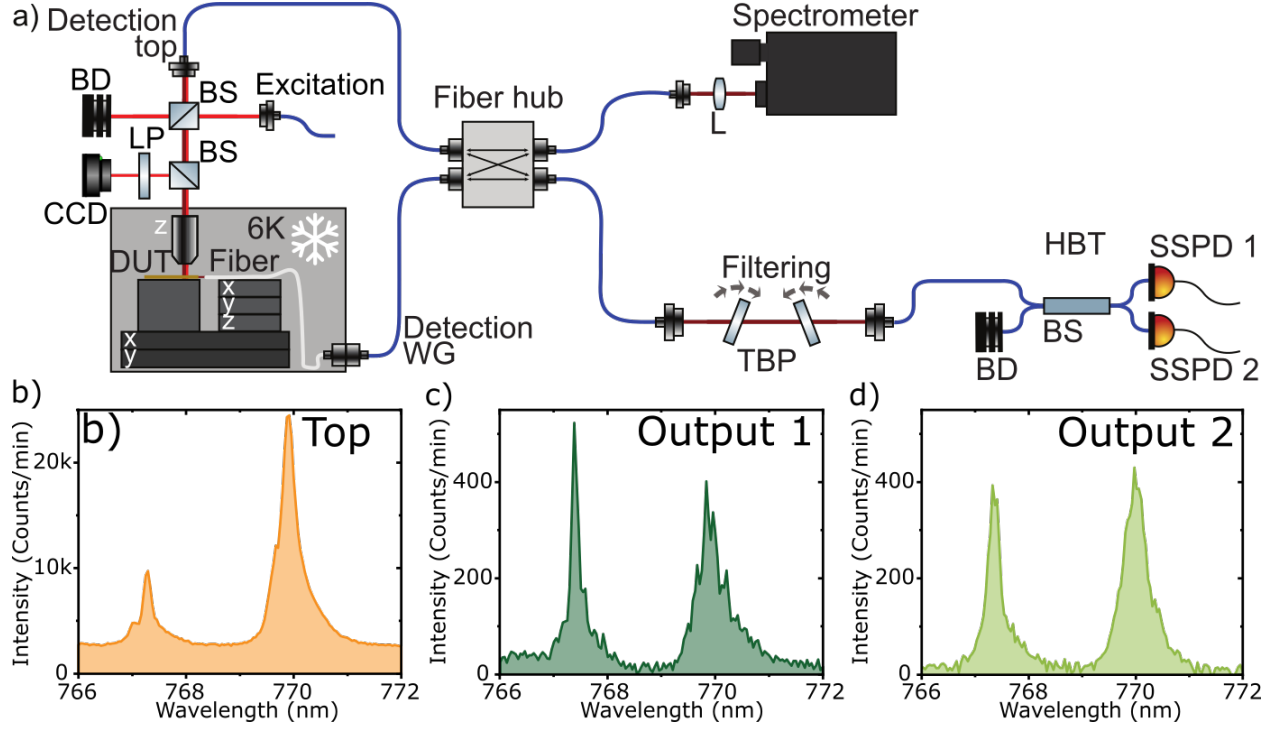


Figure 2: a) Modular setup consisting of a red laser excitation, a confocal detection path (Detection top) and a second detection path from the waveguide facet through a lensed fiber (Detection WG). In the fiber hub, the signals can be routed to the spectrometer or the Hanbury Brown and Twiss setup (HBT), which includes a free-space filtering by two tunable bandpass filters (TBP). DUT device under test; BS beam splitter; L lens; BD beam dump; SSPD superconducting single photon detector. b) Spectra from the emitter taken from top, c) through the waveguide from output 1, and d) from output 2.

414 ± 48 nW. All further measurements were performed with an excitation power of $1.4 \mu\text{W}$, located at the start of the saturation plateau for a best trade-off between signal-to-noise ratio of emission peak and background and high emission intensity.

To confirm single-photon emission, we performed a second-order autocorrelation measurement on the emitted signal of the line at 770 nm, filtered by two overlapping tunable bandpass filters (bandwidth 20 nm), using a fiber-based Hanbury Brown and Twiss setup. The detection events were time tagged and the correlation data was analyzed using ETA software³⁰ with a binning of 2048 ps.

Although the emitters were excited with a 80 MHz repetition rate pulsed laser, our second-order autocorrelation measurement, shown in Fig. 3b, resembles a measurement under a

continuous-wave laser excitation. We investigated this by measuring the emission lifetime with a lower laser repetition rate of 5 MHz (see Supplementary). Fitting the data with a double-exponential decay, we extracted a lifetime of 18.3 ± 1 ns, which is significantly longer than the separation of two consecutive excitation pulses of 12.5 ns, corresponding to a repetition rate of 80 MHz. This in turn leads to a strong overlap between neighboring peaks in the histogram, which can not be distinguished from the noise on the poisson level. Our simulation results (see Supplementary) suggest that under this circumstance, the pulsed second-order autocorrelation measurement can be treated like a continuous-wave measurement. Fitting the data with the formula given in the Supplementary yields a $g^{(2)}(0)$ of 0.168 ± 0.048 , well below 0.5 (see Fig. 3b), which demonstrates the single-photon nature of the light emission from our 2D emitter. The extracted width of the dip is 6.69 ± 0.56 ns. This value deviates from the measured lifetime using lower repetition rates. This can be explained by the high excitation power. The second-order correlation function can be described by $g^{(2)}(\tau) = 1 - (1 - g^{(2)}(0)) \exp(\tau/(\tau_l + 1/W_p))$ ³¹ with the emitter lifetime τ_l and the pump rate into the excited state W_p . This leads to a narrowing of the dip for high excitation powers, which was the case in our measurement ($1.4 \mu\text{W} = 4.4 P_{\text{sat}}$).

Additionally, we measured the second-order autocorrelation with a repetition rate of 10 MHz shown in Fig. 3c. For pulsed measurements, the second-order coherence $g^{(2)}(0)$ is given by the ratio of summed up coincidences in the center peak and average number of coincidences in the side peaks. Since the peaks still overlap in time, well-defined time windows to sum up the coincidences cannot be given. Thus, we analyzed the data following the procedure described in,³² yielding to $g^{(2)}(0)$ of 0.242 ± 0.013 .

Next, we investigated waveguide coupling of single-photon emission from 2D WSe₂ emitters. We simulate the coupling efficiency from the emitter, approximated by a dipole, into the waveguide modes (see Supplementary). By varying dipole orientation and positions along the top edge of the waveguide we calculated the dipole emission into the fundamental quasi-TE and quasi-TM waveguide modes. The unidirectional coupling efficiency to the fundamen-

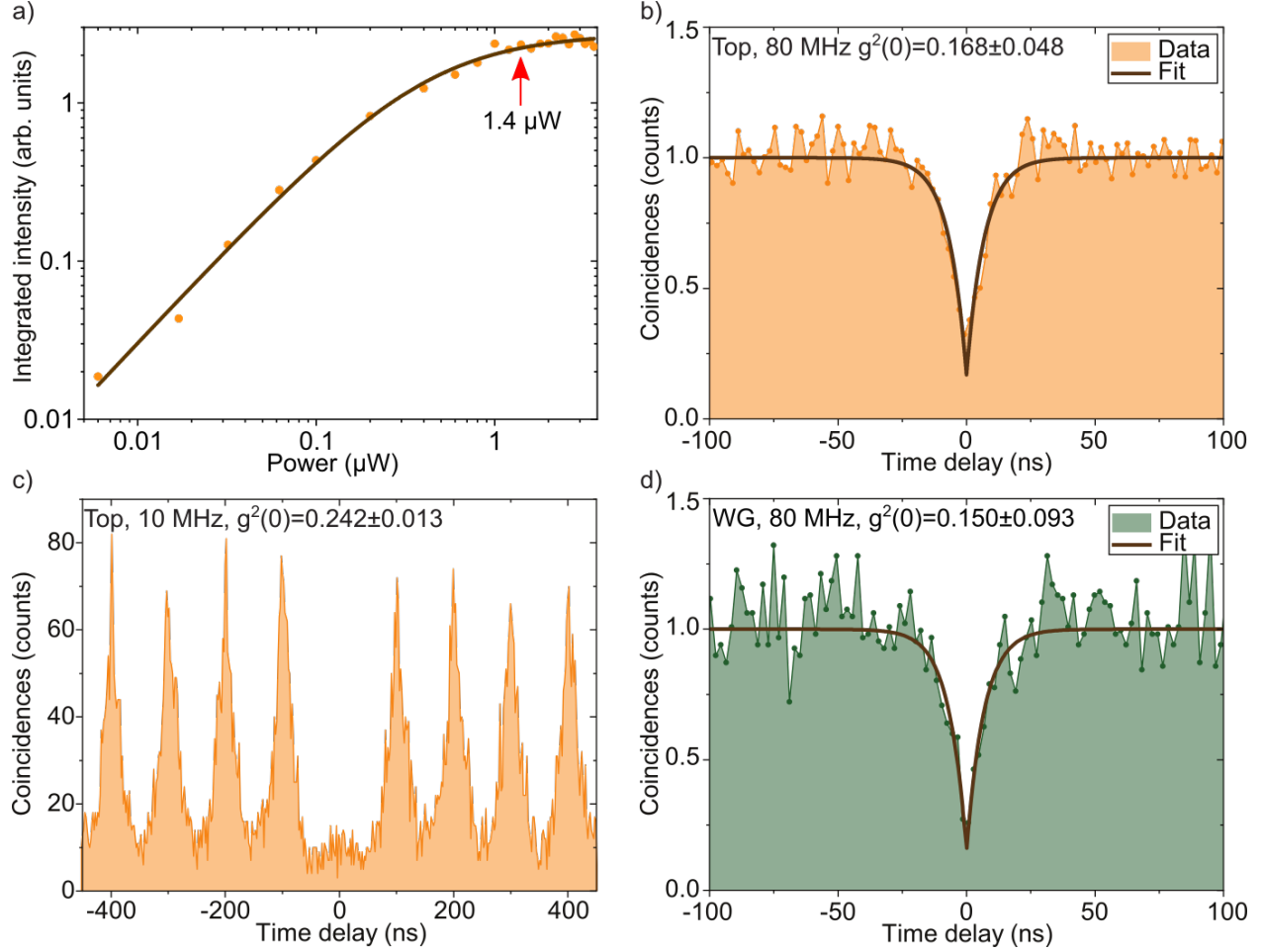


Figure 3: a) Power series with repetition rate 80 MHz. For all correlation measurements, the emitter was excited with $1.4 \mu\text{W}$, i.e. at the start of saturation plateau. b) Second-order autocorrelation measurement from top, c) with a lower repetition rate (10 MHz), and d) through the waveguide output 1.

tal modes when the dipole is located at the edge of the waveguide is, on average, 0.32%, 0.34% to the TE₀₀ and TM₀₀ mode, respectively. The coupling efficiency for all four supported modes in one direction is 3.3%. We collect this waveguide-coupled quantum emitter emission out of the waveguide using a lensed single-mode fiber mounted on an adjacent, independently movable piezoelectric stage. For all waveguide coupled measurements, the fiber was coupled to output 1, marked in Fig. 1a. We performed a second-order autocorrelation measurement through the waveguide, shown in Fig. 3d yielding $g^{(2)}(0) = 0.150 \pm 0.093$. This value shows no degradation with respect to the free-space $g^{(2)}(0)$ value, and demonstrates

strain-localized single-photon emission into a waveguide.

Although convenient to localize single emitters using local strain gradients, the emitter at the edge of the waveguide does not yield the best possible coupling efficiency to TE₀₀ and TM₀₀ mode (See simulations in the Supplementary). Thus, for our experiment it was beneficial to have slightly wider waveguides, supporting additional modes with higher field overlap at the edges of the waveguide. Ideally one then would need to adiabatically transfer the field into the fundamental mode within the waveguide, ensuring efficient fiber coupling. Another approach would be localizing the emitter at the center of the waveguide. For this geometry our simulations predict an average directional coupling efficiency of 2.48 % and 3.01 % in the TE₀₀ and TM₀₀ modes. Whereas an encapsulation of the emitter in the center of our waveguide structure with perfectly aligned dipole would result in 22 % directional coupling efficiency (only TE₀₀). The compatibility between localization scheme and optimal PIC geometry demands non-trivial solutions, which up to now are the standing challenge hindering efficient coupling. A solution may involve inducing emitters with a helium focused ion beam,³³ or point-localizing emitters using the strain arising from pillars, gaps and terminations along waveguides. Alternative methods might be dielectric screening or Moiré trapped excitons. Dielectric screening has been shown to modulate TMDs bandgap locally with the same order of magnitude as local strain but its ability to localize emitters is still to be realized.³⁴ Moiré trapped excitons appear in twisted multi-layer systems, and may provide a controllable route for emitter localization.^{35–38} Another pathway for efficient integration is coupling the emitter into a stationary cavity mode which leaks into a propagating waveguide mode. The emitter-cavity interaction results in decreased lifetime, instrumental in the presence of fast decay mechanisms, improving the brightness and the generation of indistinguishable photons. Therefore a path towards quantum PIC can take many forms where a single TMD monolayer generates many emitters, overcoming the current bottlenecks of single emitter pick-and-place methods. This can potentially be further scaled up into foundry production by full-wafer transfer with monolayers obtained by chemical vapour

deposition.³⁹

Fluctuations in the electrostatic and strain environment of individual single-photon emitters makes emitted photons spectrally differ, yielding them distinguishable and hampering quantum interference. To address this issue, spectral tuning is required, and has been demonstrated using the strain induced by piezoelectric^{40,41} and capacitive⁴² actuators, or by electric field tuning using the Stark effect.⁴³ Coupled quantum emitters are a critical part of the PIC toolbox, which also comprises on-chip excitation, filtering,^{44,45} reconfiguration,⁴⁶ and detection,⁴⁷ thus the presented 2D emitters have a road ahead of showcasing its compatibility with other building blocks towards a large-scale quantum PIC.

Quantum photonic integrated circuits provide a scalable and cost-efficient route to increasingly complex quantum systems, and constitute an enabling platform to implement applications of the quantum technologies. We have developed a hybrid deterministic integration method of single-photon emitters in 2D materials into silicon-based photonic circuits by exploiting the creation of strain-localized quantum emitters at the edges of a photonic waveguide. Our proof-of-principle structure maintains a single-photon purity of 0.150 ± 0.093 . These experimental results and proposed designs provide a new hybrid integration platform which paves the way towards large-scale quantum integrated circuits.

Acknowledgement

This project has received funding from the European Union’s Horizon 2020 research and innovation program under grant agreement No. 820423 (S2QUIP), EPSRC (EP/P029892/1) and ERC (No. 725920). C.E. acknowledges funding from the Swedish Research Council (2019-00684). K.D.J. acknowledges funding from the Swedish Research Council (VR) via the starting Grant HyQRep (Ref 2018-04812) and The Göran Gustafsson Foundation (SweTeQ). B.D.G. is supported by a Wolfson Merit Award from the Royal Society and a Chair in Emerging Technology from the Royal Academy of Engineering.

Supporting Information Available

The following files are available free of charge. The following files are available free of charge.

- Sample geometry and fabrication, experimental setup, waveguide coupling simulations, lifetime measurement, power-dependent photoluminescence measurements, simulations of second-order correlation measurements for long lifetime emitters.

Sample geometry and fabrication

The waveguide length is 2.2 mm, with a bend radius of 25 μm , and a cross-section (height \times width) of 250×800 nm. This waveguide cross-section supports 2 quasi-TE and 2 quasi-TM modes, its fundamental quasi-TE mode index being 1.72. The flake is positioned 750 μm far from one of the waveguide ends, covering a waveguide section about 20 μm long.

The sample fabrication started with a 250 nm thin stoichiometric Si_3N_4 on 3.3 μm SiO_2 on a silicon handle substrate (Rogue Valley Microdevices). The waveguides were fabricated using electron beam lithography followed by CHF_3 -based reactive ion etching, resist stripping, and sample cleaving. Flux zone grown WSe_2 crystals (from 2D semiconductors) were then exfoliated, and monolayers were identified under a microscope and transferred using a polydimethylsiloxane (PDMS) dry stamp process.²⁹

Experimental setup

The setup is shown in Fig. 2a in the main text. For all measurements, the sample was placed inside a low-vibration closed-cycle cryostat on piezoelectric xy-positioners and cooled to 6 K. For excitation, a red (638 nm) pulsed laser diode with variable repetition rate of 5 – 80 MHz was used, which was focused onto the sample using a $50\times$, $NA = 0.81$ microscope objective. The photoluminescence of the excited emitter can be detected in two ways. The proportion, which is emitted to the top, can be collected through the same microscope objective and

then coupled into a fiber. The proportion, which coupled to the Si_3N_4 waveguide can be coupled into a lensed fiber (OZOptics, 780HP, working distance $13 \pm 1 \text{ }\mu\text{m}$) at the cleaved facet of one of the waveguide ends. The lensed fiber, which was mounted on an individual xyz-positioner stack, was pre-aligned to the waveguide by sending a narrow linewidth laser at 770 nm through the fiber and maximizing the signal at the other output of the waveguide with the CCD camera through the microscope objective. The fine alignment was done by maximizing the emitter signal on the spectrometer. The fiber coupled signal can either be send to the CCD of a spectrometer (grating 600 lines/mm) or into a fiber-based Hanbury-Brown and Twiss (HBT) type setup to measure the second-order autocorrelation function. This setup consist of a 50 : 50 fiber beamsplitter connected to two superconducting single-photon detectors (Single Quantum) with efficiencies of 50%, 60%, timing jitters of 20 and 30 ps, and dark count rates of 0.006 and 0.017 cts/s. For all correlation measurements, a single line was filtered from the spectrum using two overlapping free-space tunable bandpass filters with a bandwidth of 20 nm. For excitation with a green laser (532 nm), the excitation is coupled into the setup using a dichroic longpass mirror with the edge at 695 nm (not shown in the setup). To investigate the localization of the emitters in the WSe_2 monolayer, we excite the sample with a de-focused laser (lens with $f = 300 \text{ mm}$, not shown). The emitted signal can be sent onto a CCD camera using a flip-in beamsplitter. The backscattered excitation laser is filtered with a 700 nm long pass filter.

Waveguide coupling simulations

We simulated the fabricated structure using a 3D-FDTD solver (Lumerical). The emitter is modeled as a dipole 5 nm above the waveguide. The position of the dipole is swept across the width of the waveguide in Fig. 4 ($x = 0 \text{ nm}$ at the center of the waveguide). We average over the two dipole orientations parallel to the substrate (co-linear to the waveguide and normal to the waveguide). The directional coupling emission with the emitter at the edge of the waveguide is 0.3% (3.3%) to the TE_{00} (all) modes. The maximum possible directional

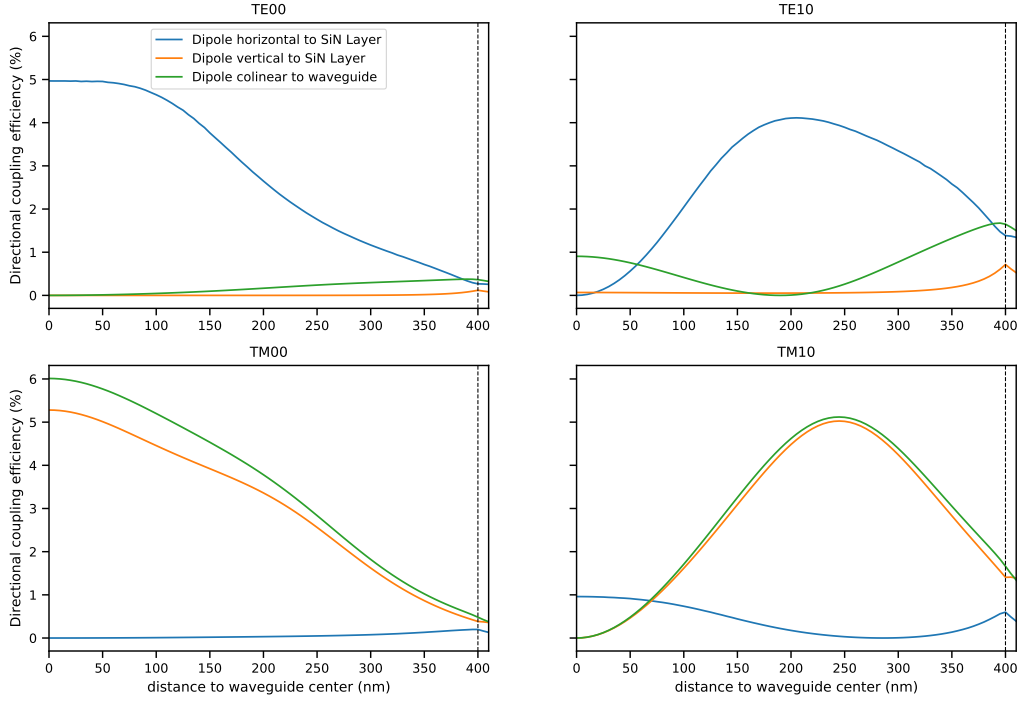


Figure 4: FDTD Simulation of the coupling efficiency to the guided modes (TE00, TE10, TM00, TM10) of the three different dipole orientations depending on the location on the waveguide. The dipole is located 5 nm above the waveguide. $x = 0$ nm is at the center of the waveguide.

coupling efficiency into the TE00 (all) mode is 2.5% (7.9%).

Lifetime measurement

To understand why our pulsed second-order correlation measurement looks like a cw measurement, we measured the lifetime of the excited state with a lower repetition rate of 5 MHz compared to the second-order correlation measurement and correlated the detected signal with the trigger from the laser in a standard time-correlated single-photon counting experiment. Figure 5 shows the data together with an double-exponential fit yielding to a lifetime of 18.3 ± 1 ns.

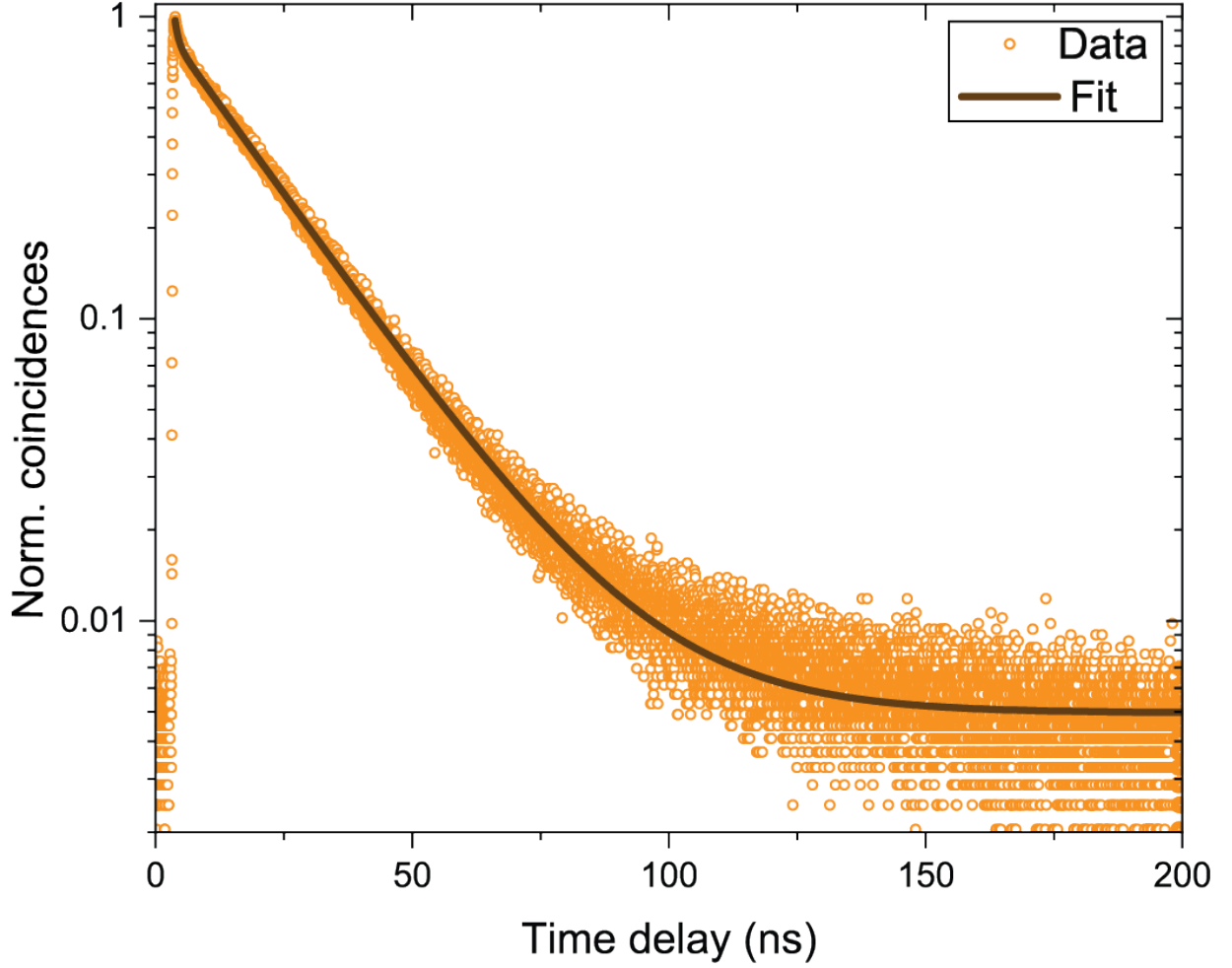


Figure 5: Lifetime measurement under red 5 MHz excitation and double-exponential fit.

Power-dependent photoluminescence measurements

A non-resonantly driven two-level system tends to saturate with increasing excitation power. Here, we investigated the behaviour for different excitation wavelengths, namely red 638 nm, with a repetition rate of 5 and 80 MHz and green 532 nm with a repetition rate of 5 MHz. In Fig. 6 we show the peak areas as a function of excitation power in a double-logarithmic plot. All data sets are fitted with $I(P) = I_{\infty} \frac{\left(\frac{P}{P_{sat}}\right)^n}{\left(\frac{P}{P_{sat}}\right)^n + 1}$ and weighted with $w_i = 1/y_i$ to compensate for the fact of less data point at low excitation energies. To compare the data sets, they are normalized with I_{∞} and P_{sat} . If the system is excited in a one-photon process, the saturation should follow the formula for $n = 1$ (orange line in Fig. 6), what is expected since the laser energy is higher than the one of the emitter. The fits are yielding to

$n = 1.09 \pm 0.16$ ($n = 1.21 \pm 0.08$) for red 5 (80) MHz and $n = 1.33 \pm 0.12$ for green 5 MHz excitation.

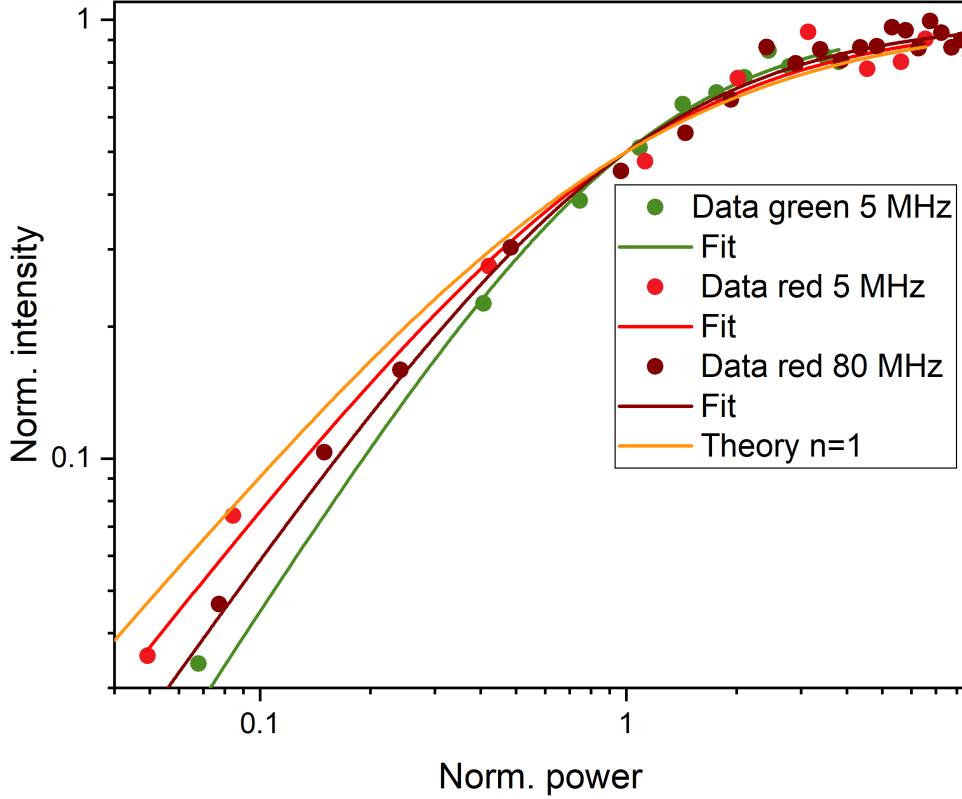


Figure 6: Peak area as a function of excitation power in a double-logarithmic plot for red (5 and 80 MHz) and green (5 MHz) excitation and the theoretical curve for a pure one-(two-photon excitation process (orange(green))).

Simulations of second-order correlation measurements for long life-time emitters

To explain why our pulsed second-order correlation measurement looks like measured under continuous-wave (cw) excitation, we simulated the resulting histogram shown in Fig. 7. Single peaks from each excitation pulse with a repetition rate of 80 MHz with a lifetime of 18.3 ns are shown in yellow together with the resulting normalized histogram in

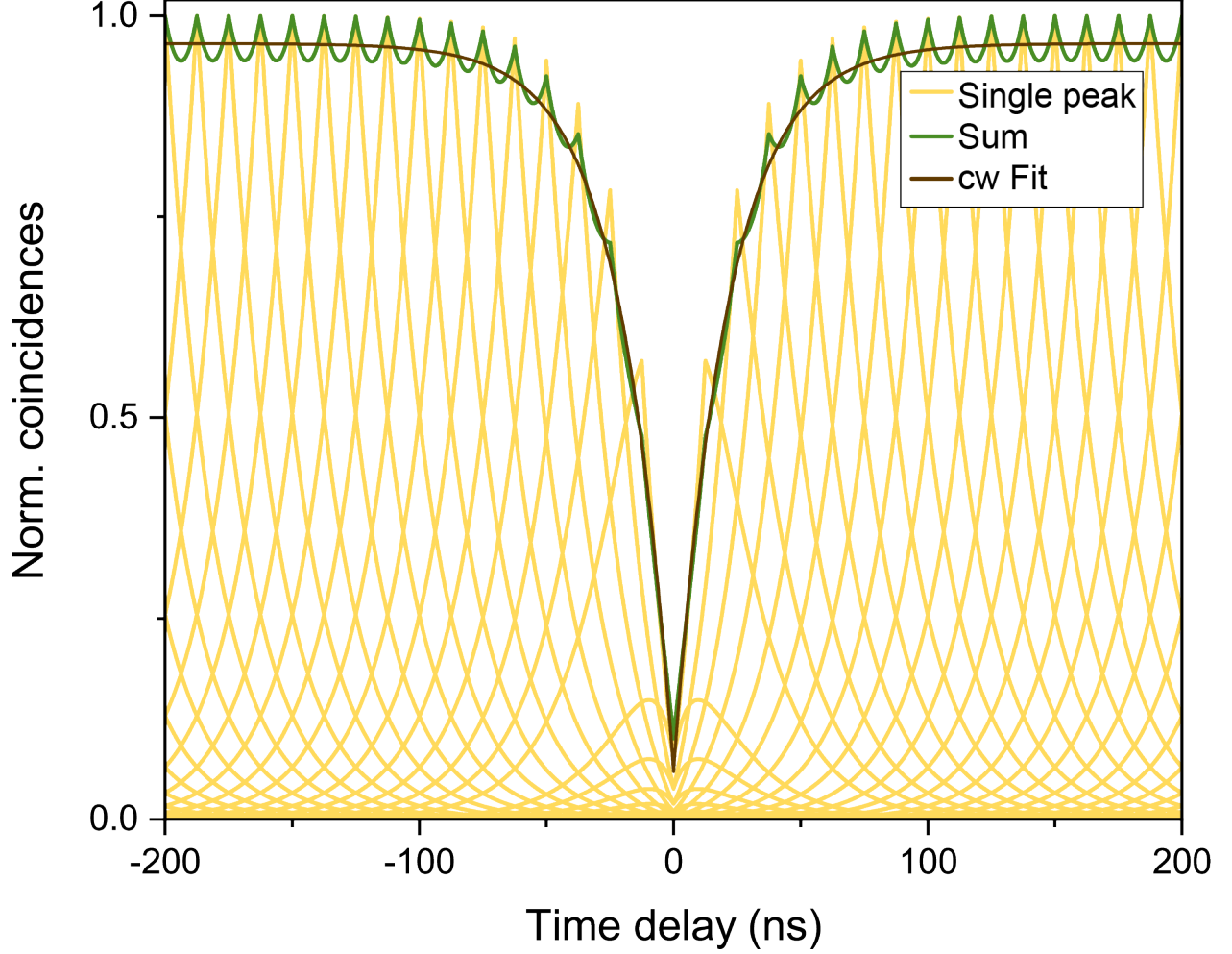


Figure 7: Simulation of a second-order correlation histogram for excitation with 80 MHz and a emitter lifetime of 18.3 ns.

green. The periodic modulations are not visible in our measurement within the noise. This strong overlap of the peaks justifies to treat the data like a cw measurement and fitted with $g^{(2)}(\tau) = B (1 - (1 - g^{(2)}(0))) \exp(\tau/\tau_0)$ with the Poisson level B and the width τ_0 , as proofed with the fit of the summed simulation peaks in brown. The deviation of the dip width of our simulation and measurements comes from the fact, that we did not take into account the pump rate in this simplified model (see main manuscript).

References

- (1) Ladd, T. D.; Jelezko, F.; Laflamme, R.; Nakamura, Y.; Monroe, C.; O’Brien, J. L. Quantum computers. *Nature* **2010**, *464*, 45–53.
- (2) Aspuru-Guzik, A.; Walther, P. Photonic quantum simulators. *Nature Physics* **2012**, *8*, 285–291.
- (3) Rudolph, T. Why I am optimistic about the silicon-photonics route to quantum computing. *APL Photonics* **2017**, *2*, 030901.
- (4) Borregaard, J.; Pichler, H.; Schöder, T.; Lukin, M. D.; Lodahl, P.; Sørensen, A. S. One-way quantum repeater based on near-deterministic photon-emitter interfaces. *arXiv:1907.05101 [quant-ph]* **2019**, arXiv: 1907.05101.
- (5) Wang, J. et al. Multidimensional quantum entanglement with large-scale integrated optics. *Science* **2018**, *360*, 285–291.
- (6) Lund-Hansen, T.; Stobbe, S.; Julsgaard, B.; Thyrrstrup, H.; Sünner, T.; Kamp, M.; Forchel, A.; Lodahl, P. Experimental Realization of Highly Efficient Broadband Coupling of Single Quantum Dots to a Photonic Crystal Waveguide. *Physical Review Letters* **2008**, *101*, 113903.
- (7) Dietrich, C. P.; Fiore, A.; Thompson, M. G.; Kamp, M.; Höfling, S. GaAs integrated quantum photonics: Towards compact and multi-functional quantum photonic integrated circuits. *Laser & Photonics Reviews* **2016**, *10*, 870–894.
- (8) Jöns, K. D.; Rengstl, U.; Oster, M.; Hargart, F.; Heldmaier, M.; Bounouar, S.; Ulrich, S. M.; Jetter, M.; Michler, P. Monolithic on-chip integration of semiconductor waveguides, beamsplitters and single-photon sources. *Journal of Physics D: Applied Physics* **2015**, *48*, 085101.

- (9) Luxmoore, I. J.; Wasley, N. A.; Ramsay, A. J.; Thijssen, A. C. T.; Oulton, R.; Hugues, M.; Kasture, S.; Achanta, V. G.; Fox, A. M.; Skolnick, M. S. Interfacing Spins in an InGaAs Quantum Dot to a Semiconductor Waveguide Circuit Using Emitted Photons. *Physical Review Letters* **2013**, *110*, 037402.
- (10) Zadeh, I. E.; Elshaari, A. W.; Jöns, K. D.; Fognini, A.; Dalacu, D.; Poole, P. J.; Reimer, M. E.; Zwiller, V. Deterministic Integration of Single Photon Sources in Silicon Based Photonic Circuits. *Nano Letters* **2016**, *16*, 2289–2294.
- (11) Kim, J.-H.; Aghaeimeibodi, S.; Richardson, C. J. K.; Leavitt, R. P.; Englund, D.; Waks, E. Hybrid Integration of Solid-State Quantum Emitters on a Silicon Photonic Chip. *Nano Letters* **2017**, *17*, 7394–7400.
- (12) Katsumi, R.; Ota, Y.; Kakuda, M.; Iwamoto, S.; Arakawa, Y. Transfer-printed single-photon sources coupled to wire waveguides. *Optica* **2018**, *5*, 691–694.
- (13) Mouradian, S. L.; Schröder, T.; Poitras, C. B.; Li, L.; Goldstein, J.; Chen, E. H.; Walsh, M.; Cardenas, J.; Markham, M. L.; Twitchen, D. J.; Lipson, M.; Englund, D. Scalable Integration of Long-Lived Quantum Memories into a Photonic Circuit. *Physical Review X* **2015**, *5*, 031009.
- (14) Stanford, M. G.; Rack, P. D.; Jariwala, D. Emerging nanofabrication and quantum confinement techniques for 2D materials beyond graphene. *npj 2D Materials and Applications* **2018**, *2*, 1–15.
- (15) Liu, X.; Hersam, M. C. 2D materials for quantum information science. *Nature Reviews Materials* **2019**, *4*, 669–684.
- (16) Tonndorf, P.; Schmidt, R.; Schneider, R.; Kern, J.; Buscema, M.; Steele, G. A.; Castellanos-Gomez, A.; Zant, H. S. J. v. d.; Vasconcellos, S. M. d.; Bratschitsch, R. Single-photon emission from localized excitons in an atomically thin semiconductor. *Optica* **2015**, *2*, 347–352.

- (17) Kumar, S.; Kaczmarczyk, A.; Gerardot, B. D. Strain-Induced Spatial and Spectral Isolation of Quantum Emitters in Mono- and Bilayer WSe₂. *Nano Letters* **2015**, *15*, 7567–7573.
- (18) Srivastava, A.; Sidler, M.; Allain, A. V.; Lembke, D. S.; Kis, A.; Imamoğlu, A. Optically active quantum dots in monolayer WSe₂. *Nature Nanotechnology* **2015**, *10*, 491–496.
- (19) He, Y.-M.; Clark, G.; Schaibley, J. R.; He, Y.; Chen, M.-C.; Wei, Y.-J.; Ding, X.; Zhang, Q.; Yao, W.; Xu, X.; Lu, C.-Y.; Pan, J.-W. Single quantum emitters in monolayer semiconductors. *Nature Nanotechnology* **2015**, *10*, 497–502.
- (20) Koperski, M.; Nogajewski, K.; Arora, A.; Cherkez, V.; Mallet, P.; Veuillen, J.-Y.; Marcus, J.; Kossacki, P.; Potemski, M. Single photon emitters in exfoliated WSe₂ structures. *Nature Nanotechnology* **2015**, *10*, 503–506.
- (21) Chakraborty, C.; Kinnischtzke, L.; Goodfellow, K. M.; Beams, R.; Vamivakas, A. N. Voltage-controlled quantum light from an atomically thin semiconductor. *Nature Nanotechnology* **2015**, *10*, 507–511.
- (22) Branny, A.; Kumar, S.; Proux, R.; Gerardot, B. D. Deterministic strain-induced arrays of quantum emitters in a two-dimensional semiconductor. *Nature Communications* **2017**, *8*, 1–7.
- (23) Palacios-Berraquero, C.; Kara, D. M.; Montblanch, A. R.-P.; Barbone, M.; Latawiec, P.; Yoon, D.; Ott, A. K.; Loncar, M.; Ferrari, A. C.; Atatüre, M. Large-scale quantum-emitter arrays in atomically thin semiconductors. *Nature Communications* **2017**, *8*, 1–6.
- (24) White, D.; Branny, A.; Chapman, R. J.; Picard, R.; Brotons-Gisbert, M.; Boes, A.; Peruzzo, A.; Bonato, C.; Gerardot, B. D. Atomically-thin quantum dots integrated with lithium niobate photonic chips [Invited]. *Optical Materials Express* **2019**, *9*, 441–448.

- (25) Blauth, M.; Jürgensen, M.; Vest, G.; Hartwig, O.; Prechtel, M.; Cerne, J.; Finley, J. J.; Kaniber, M. Coupling Single Photons from Discrete Quantum Emitters in WSe₂ to Lithographically Defined Plasmonic Slot Waveguides. *Nano Letters* **2018**, *18*, 6812–6819.
- (26) Tonndorf, P.; Del Pozo-Zamudio, O.; Gruhler, N.; Kern, J.; Schmidt, R.; Dmitriev, A. I.; Bakhtinov, A. P.; Tartakovskii, A. I.; Pernice, W.; Michaelis de Vasconcellos, S.; Bratschitsch, R. On-Chip Waveguide Coupling of a Layered Semiconductor Single-Photon Source. *Nano Letters* **2017**, *17*, 5446–5451.
- (27) Peyskens, F.; Chakraborty, C.; Muneeb, M.; Thourhout, D. V.; Englund, D. Integration of single photon emitters in 2D layered materials with a silicon nitride photonic chip. *Nature Communications* **2019**, *10*, 1–7.
- (28) Kim, S.; Duong, N. M. H.; Nguyen, M.; Lu, T.-J.; Kianinia, M.; Mendelson, N.; Solntsev, A.; Bradac, C.; Englund, D. R.; Aharonovich, I. Integrated on Chip Platform with Quantum Emitters in Layered Materials. *Advanced Optical Materials* *0*, 1901132.
- (29) Castellanos-Gomez, A.; Buscema, M.; Molenaar, R.; Singh, V.; Janssen, L.; Zant, H. S. J. v. d.; Steele, G. A. Deterministic transfer of two-dimensional materials by all-dry viscoelastic stamping. *2D Materials* **2014**, *1*, 011002.
- (30) Extensible Timetag Analyzer. 2019; <https://github.com/timetag/ETA>, original-date: 2018-03-13T19:49:47Z.
- (31) Michler, P.; Imamoglu, A.; Mason, M. D.; Carson, P. J.; Strouse, G. F.; Buratto, S. K. Quantum correlation among photons from a single quantum dot at room temperature. *Nature* **2000**, *406*, 968–970.
- (32) Schöll, E.; Hanschke, L.; Schweickert, L.; Zeuner, K. D.; Reindl, M.; Covre da Silva, S. F.; Lettner, T.; Trotta, R.; Finley, J. J.; Müller, K.; Rastelli, A.; Zwiller, V.;

- Jöns, K. D. Resonance Fluorescence of GaAs Quantum Dots with Near-Unity Photon Indistinguishability. *Nano Letters* **2019**, *19*, 2404–2410.
- (33) Klein, J. et al. Site-selectively generated photon emitters in monolayer MoS₂ via local helium ion irradiation. *Nature Communications* **2019**, *10*, 1–8.
- (34) Raja, A. et al. Coulomb engineering of the bandgap and excitons in two-dimensional materials. *Nature Communications* **2017**, *8*, 1–7.
- (35) Tran, K. et al. Evidence for moiré excitons in van der Waals heterostructures. *Nature* **2019**, *567*, 71–75.
- (36) Seyler, K. L.; Rivera, P.; Yu, H.; Wilson, N. P.; Ray, E. L.; Mandrus, D. G.; Yan, J.; Yao, W.; Xu, X. Signatures of moiré-trapped valley excitons in MoSe₂/WSe₂ heterobilayers. *Nature* **2019**, *567*, 66–70.
- (37) Brotons-Gisbert, M.; Baek, H.; Molina-Sánchez, A.; Scerri, D.; White, D.; Watanabe, K.; Taniguchi, T.; Bonato, C.; Gerardot, B. D. Spin-layer locking of interlayer valley excitons trapped in moiré potentials. *arXiv:1908.03778 [cond-mat]* **2019**, arXiv: 1908.03778.
- (38) Baek, H.; Brotons-Gisbert, M.; Koong, Z. X.; Campbell, A.; Rambach, M.; Watanabe, K.; Taniguchi, T.; Gerardot, B. D. Highly tunable quantum light from moiré trapped excitons. *arXiv:2001.04305 [cond-mat]* **2020**, arXiv: 2001.04305.
- (39) Quellmalz, A.; Wang, X.; Wagner, S.; Lemme, M.; Gylfason, K. B.; Roxhed, N.; Stemme, G.; Niklaus, F. Wafer-Scale Transfer of Graphene by Adhesive Wafer Bonding. 2019 IEEE 32nd International Conference on Micro Electro Mechanical Systems (MEMS). 2019; pp 257–259, ISSN: 1084-6999.
- (40) Iff, O.; Tedeschi, D.; Martín-Sánchez, J.; Moczala-Dusanowska, M.; Tongay, S.; Yumigeta, K.; Taboada-Gutiérrez, J.; Savaresi, M.; Rastelli, A.; Alonso-González, P.;

- Höfling, S.; Trotta, R.; Schneider, C. Strain-Tunable Single Photon Sources in WSe₂ Monolayers. *Nano Letters* **2019**, *19*, 6931–6936.
- (41) Kim, H.; Moon, J. S.; Noh, G.; Lee, J.; Kim, J.-H. Position and Frequency Control of Strain-Induced Quantum Emitters in WSe₂ Monolayers. *Nano Letters* **2019**, *19*, 7534–7539.
- (42) Grosso, G.; Moon, H.; Lienhard, B.; Ali, S.; Efetov, D. K.; Furchi, M. M.; Jarillo-Herrero, P.; Ford, M. J.; Aharonovich, I.; Englund, D. Tunable and high-purity room temperature single-photon emission from atomic defects in hexagonal boron nitride. *Nature Communications* **2017**, *8*, 1–8.
- (43) Noh, G.; Choi, D.; Kim, J.-H.; Im, D.-G.; Kim, Y.-H.; Seo, H.; Lee, J. Stark Tuning of Single-Photon Emitters in Hexagonal Boron Nitride. *Nano Letters* **2018**, *18*, 4710–4715.
- (44) Elshaari, A. W.; Zadeh, I. E.; Fognini, A.; Reimer, M. E.; Dalacu, D.; Poole, P. J.; Zwiller, V.; Jöns, K. D. On-chip single photon filtering and multiplexing in hybrid quantum photonic circuits. *Nature Communications* **2017**, *8*, 379.
- (45) Zhou, X.; Uppu, R.; Liu, Z.; Papon, C.; Schott, R.; Wieck, A. D.; Ludwig, A.; Lodahl, P.; Midolo, L. On-chip nanomechanical filtering of quantum-dot single-photon sources. *arXiv:1910.05785 [physics, physics:quant-ph]* **2019**, arXiv: 1910.05785.
- (46) Papon, C.; Zhou, X.; Thyrrstrup, H.; Liu, Z.; Stobbe, S.; Schott, R.; Wieck, A. D.; Ludwig, A.; Lodahl, P.; Midolo, L. Nanomechanical single-photon routing. *Optica* **2019**, *6*, 524–530.
- (47) Ferrari, S.; Schuck, C.; Pernice, W. Waveguide-integrated superconducting nanowire single-photon detectors. *Nanophotonics* **2018**, *7*, 1725–1758.